Articles

Bimetallic Assemblies $[Ni(L)_2]_3[Fe(CN)_6]X_2$ (L = Ethylenediamine, Trimethylenediamine; X = PF_6^-, ClO_4^-) with a Three-Dimensional Network Extended through $Fe^{II}-CN-Ni^{II}$ Linkages

Nobuo Fukita,[†] Masaaki Ohba,*,[†] Hisashi Ōkawa,*,[†] Kenji Matsuda,[‡] and Hiizu Iwamura[‡]

Department of Chemistry, Faculty of Science, Kyushu University, Hakozaki, Higashi-ku, Fukuoka 812, Japan, and Institute for Fundamental Research of Organic Chemistry, Kyushu University, Fukuoka 812, Japan

Received August 29, 1997

Three-dimensional cyanide-bridged bimetallic assemblies $[Ni(L)_2]_3[Fe^{II}(CN)_6]X_2$ ((L, X) = (ethylenediamine (en), PF_6^-) (**1**), (trimethylenediamine (tn), PF_6^-) (**2**), (tn, ClO_4^-) (**3**)) were synthesized and structurally characterized. Compounds **1**−**3** crystallize in the trigonal system of the space group $R\bar{3}$ with $a = b = 13.743(1)$ Å, $c = 17.802(2)$ Å, and $Z = 3$ for **1**, $a = b = 14.588(1)$ Å, $c = 17.050(2)$ Å, and $Z = 3$ for **2**, and $a = b = 14.337(2)$ Å, $c = 17.294(4)$ Å, and $Z = 3$ for **3**. All the assemblies have an isotropic three-dimensional network structure extended through Fe−CN−Ni linkages. The network is based on a cube formed by 8 $[Fe(CN)_6]^{4-}$ anions at the corners and 12 $[Ni(L)_2]^{2+}$ cations at the edges. Two hexafluorophosphate or perchlorate anions are located in the cavity of the Fe_8Ni_{12} cube and align along a diagonal axis that coincides with the *c* axis. Magnetic measurements show a ferromagnetic interaction between the nearest Ni^{II} ions through the diamagnetic Fe^{II} ion.

Introduction

Recently, there has been a growing interest in coordination polymers having a two- (2-D) or three-dimensional (3-D) structure because of the unique physicochemical properties arising in the bulk of these systems.[1−43] In particular, much effort has been made for the design of highly ordered structures with paramagnetic metal centers in order to provide molecular-

[†] Department of Chemistry.
[‡] Institute for Fundamental Research of Organic Chemistry.

(1) Hoskins, B. F.; Robson, R. *J. Am. Chem. Soc.* **1990**, *112*, 1546.
(2) Fujita, M.; Kwon, Y. J.; Washizu, S.; Ogura, K. *J. Am. Chem. Soc.* **1994**, *116*, 1151.
(3) MacGillivray, L. R.; Subramanian, S.; Zaworotko, M. J. *J. Chem. Soc., Chem. Commun.* **1994**, 1325.
(4) Abrahams, B. F.; Hardie, M. D.; Hoskins, B. F.; Robson, R.; Sutherland, E. E. *J. Chem. Soc., Chem. Commun.* **1994**, 1049.
(5) Soma, T.; Yuge, T.; Iwamoto, T. *Angew. Chem., Int. Ed. Engl.* **1994**, *33*, 1665.
(6) Subramanian, S.; Zaworotko, M. J. *Angew. Chem., Int. Ed. Engl.* **1995**, *34*, 2127.
(7) Carlucci, L.; Ciani, G.; Proserpio, D. M.; Sironi, A. *J. Am. Chem. Soc.* **1995**, *117*, 1677.
(8) Carlucci, L.; Ciani, G.; Proserpio, D. M.; Sironi, A. *Angew. Chem., Int. Ed. Engl.* **1995**, *34*, 1895.
(9) Ohba, M.; Maruono, N.; Ōkawa, H.; Enoki, T.; Latour, J. M. *J. Am. Chem. Soc.* **1994**, *116*, 11566.
(10) Ohba, M.; Ōkawa, H.; Ito, T.; Ohto, A. *J. Chem. Soc., Chem. Commun.* **1995**, 1545.
(11) Ōkawa, H.; Ohba, M. In *Molecule-Based Magnetic Materials*; Turnbull, M. M., Sugimoto, T., Thompson, L. K., Eds.; ACS Symposium Series 644; American Chemical Society: Washington, DC, 1996; p 319.
(12) Ohba, M.; Ōkawa, H. *Mol. Cryst. Liq. Cryst.* **1996**, *286*, 101.
(13) Ohba, M.; Fukita, N.; Ōkawa, H. *J. Am. Chem. Soc.* **1997**, *119*, 1011.
(14) Ohba, M.; Fukita, N.; Ōkawa, H. *J. Chem. Soc., Dalton Trans.* **1997**, 1733.
(15) Ohba, M.; Shinzato, H. Unpublished result.
(16) Miyasaka, H.; Matsumoto, N.; Ōkawa, H.; Re, N.; Gallo, E.; Floriani, C. *Angew. Chem., Int. Ed. Engl.* **1995**, *34*, 1446.
(17) Miyasaka, H.; Matsumoto, N.; Ōkawa, H.; Re, N.; Gallo, E.; Floriani, C. *J. Am. Chem. Soc.* **1996**, *118*, 981.
(18) Re, N.; Gallo, E.; Floriani, C.; Miyasaka, H.; Matsumoto, N. *Inorg. Chem.* **1996**, *35*, 5964.
(19) Re, N.; Gallo, E.; Floriani, C.; Miyasaka, H.; Matsumoto, N. *Inorg. Chem.* **1996**, *35*, 6004.
(20) El Fallah, M.; Rentschler, E.; Caneschi, A.; Sessoli, R.; Gatteschi, D. *Angew. Chem., Int. Ed. Engl.* **1996**, *35*, 1947.
(21) Farlay, S.; Mallah, T.; Vaissermann, J.; Bartolome, F.; Veillet, P.; Verdaguer, M. *Chem. Commun.* **1996**, 2481.
(22) Kahn, O. *Adv. Inorg. Chem.* **1995**, *43*, 179.
(23) Stumpf, H. O.; Ouahab, L.; Pei, Y.; Grandjean, D.; Kahn, O. *Science* **1993**, *261*, 447.
(24) Inoue, K.; Iwamura, H. *J. Am. Chem. Soc.* **1994**, *116*, 3137.
(25) Inoue, K.; Hayamizu, T.; Iwamura, H.; Hashizume, D.; Ohashi, Y. *J. Am. Chem. Soc.* **1996**, *118*, 1803.
(26) Schwarz, P.; Siebel, E.; Fischer, R. D.; Apperley, D. C.; Davies, N. A.; Harris, R. K. *Angew. Chem., Int. Ed. Engl.* **1995**, *34*, 1197.
(27) Lu, J.; Harrison, W. T. A.; Jacobson, A. J. *Angew. Chem., Int. Ed. Engl.* **1995**, *34*, 2557.
(28) Lu, J.; Harrison, W. T. A.; Jacobson, A. J. *Inorg. Chem.* **1996**, *35*, 4271.
(29) Herren, F.; Fischer, P.; Ludi, A.; Hälg, W. *Inorg. Chem.* **1980**, *19*, 956.
(30) Klenze, H.; Kanellalopulos, B.; Tragester, G.; Eysel, H. H. *J. Chem. Phys.* **1980**, *72*, 5819.
(31) Griebler, W. D.; Babel, D. *D. Z. Naturforsch.* **1982**, *87b*, 832.
(32) Gadet, V.; Bujoli-Doeuff, M.; Force, L.; Verdaguer, M.; Malkhi, K. El, Deroy, A.; Besse, J. P.; Chappert, C.; Veillet, P.; Renard, J. P.; Beauvillain, P. In *Molecular Magnetic Materials*; Gatteschi, D., et al., Eds.; NATO ASI Series 198; Kluwer: Dordrecht, The Netherlands, 1990; p 281.
(33) Gadet, V.; Mallah, T.; Castro, I.; Verdaguer, M. *J. Am. Chem. Soc.* **1992**, *114*, 9213.
(34) Mallah, S.; Thiebaut, S.; Verdaguer, M.; Veillet, P. *Science* **1993**, *262*, 1554.
(35) Ently, W. R.; Girolani, G. S. *Science* **1995**, *268*, 397.
(36) Ently, W. R.; Girolani, G. S. *Inorg. Chem.* **1994**, *33*, 5165.
(37) Ferlay, S.; Mallah, T.; Ouahés, R.; Veillet, P.; Verdaguer, M. *Nature* **1995**, *378*, 701.
(38) Kahn, O. *Nature* **1995**, *378*, 667.

S0020-1669(97)01116-6 CCC: $15.00
Published on Web 01/31/1998

Chart 1

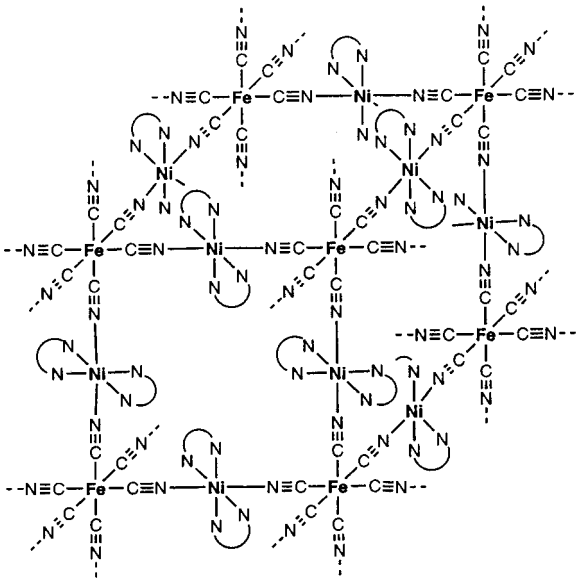

based magnets exhibiting spontaneous magnetization.[9−43] It is known that hexacyanometalate ions, $[M(CN)_6]^{n-}$, act as good building blocks to provide bimetallic assemblies such as Prussian blue, $Fe^{III}_4[Fe^{II}(CN)_6]_3 \cdot nH_2O$. Prussian blue and its analogues form a family of magnetic materials, and a high T_C or T_N is reported for some of these assemblies.[30−41] However, magneto−structural correlation of these high T_C or T_N compounds remains unclear because of the difficulty of crystallization. To get structural information for a deeper insight into the mechanism of the magnetic interaction throughout a network structure, we have initiated the study of bimetallic assemblies derived from a hexacyanometalate ion and a four-coordinate bis(diamine)-nickel(II) complex $[Ni(L)_2]^{2+}$ (L = diamine ligand). The use of $[Ni(L)_2]^{2+}$ instead of the simple metal ion in the Prussian blue analogues reduces the complexity in stereochemistry of the resulting bimetallic assemblies because the geometry about the nickel in the assemblies is invariably six-coordinate together with two cyano nitrogens. Previously, we reported the crystal structures of $[Ni(en)_2]_3[Fe(CN)_6]_2 \cdot 2H_2O$ (en = ethylenediamine),[9,14] $PPh_4[Ni(pn)_2][Fe(CN)_6]H_2O$ (pn = 1,2-propanediamine),[11] $[Ni(L)_2]_2[Fe(CN)_6]X \cdot nH_2O$ (L = pn, 1,1-dimethylethylenediamine (1,1-dmen); X = ClO_4^-, PF_6^-, *etc.*),[10−13] and $[Ni(N\text{-}men)_2]_3[Fe(CN)_6]_2 \cdot nH_2O$ (N-men = *N*-methylethylenediamine).[15] They have a 1-D rope-ladder-like chain structure, a 1-D zigzag chain structure, a 2-D square sheet structure, and a 2-D honeycomb sheet structure, respectively. These bimetallic assemblies can be rationally prepared by the reaction of $[M(CN)_6]^{3-}$ and $[Ni(L)_3]^{2+}$ in the respective stoichiometry, in the absence or presence of an appropriate counterion, and by the choice of the diamine ligand. However, the bimetallic assemblies so far obtained are limited to those of a 1-D or 2-D network.

Our next target is 3-D bimetallic assemblies constructed from $[M(CN)_6]^{n-}$ and $[Ni(L)_2]^{2+}$ ions (see Chart 1). In this study, we have obtained new types of bimetallic assemblies $[Ni(L)_2]_3[Fe(CN)_6]X_2$ (L = en, tn; X = PF_6^-, ClO_4^-) using hexacyanoferrate(II), $[Fe(CN)_6]^{4-}$, as the building block. Their crystal structures were determined by X-ray crystallography revealing a 3-D network structure extended by $Fe^{II}-CN-Ni^{II}$ linkages. Cryomagnetic properties of the assemblies are also reported.

Experimental Section

Physical Measurements. Elemental analyses of carbon, hydrogen, and nitrogen were obtained at the Service Center of Elemental Analysis of Kyushu University. Metal (iron and nickel) analyses were made on a Shimadzu AA-680 atomic absorption/flame emission spectrophotometer. Infrared spectra were measured on a JASCO IR-810 spectrophotometer using KBr disks. Magnetic susceptibilities were measured by a Quantum Design MPMS-5S SQUID susceptometer. Diamagnetic corrections were made using Pascal's constants. Effective magnetic moments were calculated by the equation $\mu_{eff} = 2.828(\chi_M T)^{1/2}$, where χ_M is the molar magnetic susceptibility corrected for diamagnetism of the constituting atoms. Field dependencies of magnetization were determined on the same susceptometer under an applied magnetic field up to 50 kG.

Preparations. The Ni^{II} component complexes $[Ni(L)_3]X_2$ (L = en, tn; X = PF_6^-, ClO_4^-) were prepared according to the literature method.[44] $K_4[Fe(CN)_6]$ (Nakalai Tesque Inc.) was of reagent grade and used as purchased.

$[Ni(en)_2]_3[Fe(CN)_6](PF_6)_2$ (1). $[Ni(en)_3](PF_6)_2$ (156 mg, 0.33 mmol) was dissolved in 10 cm^3 of water. To this solution was added an aqueous solution (10 cm^3) of $K_4[Fe(CN)_6]$ (47 mg, 0.11 mmol) at room temperature, and the resulting purple solution was allowed to stand to form purple cubic crystals. They were collected by suction filtration, washed with water, and dried *in vacuo* over P_2O_5. All the operations for the synthesis were carried out in the dark to avoid the decomposition of $K_4[Fe(CN)_6]$. Yield: 74 mg (65%). Anal. Calcd for $C_{18}H_{48}F_{12}FeN_{18}Ni_3P_2$: C, 20.82; H, 4.66; N, 24.28; Fe, 5.4; Ni, 17.0. Found: C, 20.90; H, 4.66; N, 24.39; Fe, 4.9; Ni, 16.8. IR (cm^{-1}, KBr disk): ν_{CN} 2060.

$[Ni(tn)_2]_3[Fe(CN)_6](PF_6)_2$ (2). This assembly was prepared as purple cubic crystals in a way similar to that of **1**, except for the use of $[Ni(tn)_3](PF_6)_2$ instead of $[Ni(en)_3](PF_6)_2$. Yield: 81 mg (65%). Anal. Calcd for $C_{24}H_{60}F_{12}FeN_{18}Ni_3P_2$: C, 25.68; H, 5.39; N, 22.46; Fe, 5.0; Ni, 15.7. Found: C, 25.91; H, 5.38; N, 22.34; Fe, 4.9; Ni, 15.5. IR (cm^{-1}, KBr disk): ν_{CN} 2060.

$[Ni(tn)_2]_3[Fe(CN)_6](ClO_4)_2$ (3). This was prepared as purple cubic crystals in a way similar to that of **1** using $[Ni(tn)_3](ClO_4)_2$ instead of $[Ni(en)_3](PF_6)_2$. Yield: 27 mg (24%). Anal. Calcd for $C_{24}H_{60}Cl_2FeN_{18}Ni_3O_8$: C, 27.94; H, 5.86; N, 24.44; Fe, 5.4; Ni, 17.1. Found: C, 27.84; H, 5.86; N, 24.45; Fe, 5.2; Ni, 17.4. IR (cm^{-1}, KBr disk): ν_{CN} 2060.

Caution! *Perchlorate salts are potentially explosive and should be handled in small quantities.*

X-ray Structural Analyses. All the measurements were made on a Rigaku AFC7R diffractometer with graphite-monochromated Mo Kα radiation (λ = 0.710 69 Å) and a 12 kW rotating anode generator. The data were collected at 20 ± 1 °C using the $\omega-2\theta$ scan technique to a maximum 2θ value of 50.0° at a scan speed 16.0°/min (in ω). The weak reflections ($I < 10.0\sigma(I)$) were rescanned (maximum of 4 scans), and the counts were accumulated to ensure good counting statistics. Stationary background counts were recorded on each side of the reflection. The ratio of peak counting time to background counting time was 2:1. The cell parameters of **1**−**3** were determined by 25 reflections in the 2θ range of $29.27° \le 2\theta \le 29.75°$, $29.14° \le 2\theta \le 29.96°$, and $29.03° \le 2\theta \le 29.92°$, respectively. The octant measured was $\pm h,+k,+l$. The intensities of the representative reflections were measured after every 150 reflections. Over the course of the data collection, the standards for **1** and **2** decreased by 0.3 and 16.9%, respectively, and the standards of **3** increased by 0.2%. A linear correction factor was applied to the data to account for these phenomena. Intensity data were corrected for Lorentz and polarization effects.

(39) Sato, O.; Iyoda, T.; Fujishima, A.; Hashimoto, K. *Science* **1996**, *271*, 49.
(40) Verdaguer, M. *Science* **1996**, *272*, 698.
(41) Sato, O.; Iyoda, T.; Fujishima, A.; Hashimoto, K. *Science* **1996**, *272*, 704.
(42) Arrio, M.-A.; Sainctavit, P.; Moulin, C.; Mallah, T.; Verdaguer, M.; Pellegrin, E.; Chen, C. *J. Am. Chem. Soc.* **1996**, *118*, 6422.
(43) Dumbar, K. R.; Heintz, R. A. *Prog. Inorg. Chem.* **1997**, *45*, 283.
(44) Werner, A. *Z. Anorg. Chem.* **1899**, *21*, 210.

Table 1 Crystal Parameters for **1**−**3**

	1	**2**	**3**
fw	1038.57	1122.73	1031.71
space group	$R\bar{3}$(No. 148)	$R\bar{3}$(No. 148)	$R\bar{3}$(No. 148)
$a = b$/Å	13.743(1)	14.588(1)	14.337(2)
c/Å	17.802(2)	17.050(2)	17.294(4)
V/Å^3	2911.8(4)	3142.3(6)	3078(1)
Z	3	3	3
D_c/g cm^{-3}	1.777	1.780	1.669
μ(Mo Kα)/cm^{-1}	19.81	18.43	18.98
R^a	0.035	0.019	0.024
$R_w{}^b$	0.034	0.019	0.022

^{a} $R = \sum||F_o| - |F_c||/\sum|F_o|$. ^{b} $R_w = [(\sum(|F_o| - |F_c|)^2/\sum F_o^2]^{1/2}$.

Table 2. Atomic Coordinates and Equivalent Isotropic Thermal Parameters (Å^2) of Non-Hydrogen Atoms in $[Ni(en)_2]_3[Fe(CN)_6](PF_6)_2$ (**1**)

atom	x	y	z	B(eq)
Ni	$^1/_2$	$-^1/_2$	$-^1/_2$	2.35(2)
Fe	0.6667	−0.6667	−0.6667	1.33(1)
P	1.0000	0	−0.3616(1)	3.31(3)
F(1)	1.1014(2)	0.0176(3)	−0.3095(2)	6.56(9)
F(2)	1.0171(3)	−0.0847(3)	−0.4102(2)	8.1(1)
N(1)	0.6199(3)	−0.5151(3)	−0.5647(2)	3.47(9)
N(2)	0.6061(3)	−0.4463(3)	−0.4064(2)	3.7(1)
N(3)	0.5823(3)	−0.3254(3)	−0.5196(2)	3.5(1)
C(1)	0.6401(3)	−0.5694(3)	−0.6039(2)	2.03(8)
C(2)	0.6812(5)	−0.3285(5)	−0.4097(3)	7.0(2)
C(3)	0.6701(5)	−0.2686(5)	−0.4665(4)	8.7(2)

Table 3. Atomic Coordinates and Equivalent Isotropic Thermal Parameters (Å^2) of Non-Hydrogen Atoms in $[Ni(tn)_2]_3[Fe(CN)_6](PF_6)_2$ (**2**)

atom	x	y	z	B(eq)
Ni	$^1/_2$	$-^1/_2$	$-^1/_2$	1.56(1)
Fe	0.6667	−0.6667	−0.6667	1.20(1)
P	1.0000	0	−0.3597(1)	2.11(1)
F(1)	1.0150(1)	−0.0812(1)	−0.4121(1)	3.93(3)
F(2)	0.9194(1)	−0.0960(1)	−0.3049(1)	3.81(3)
N(1)	0.6144(1)	−0.5238(1)	−0.5637(1)	2.16(4)
N(2)	0.4235(1)	−0.6639(1)	−0.4753(1)	2.33(4)
N(3)	0.4143(1)	−0.5369(2)	−0.6060(1)	2.29(4)
C(1)	0.6374(1)	−0.5754(1)	−0.6017(1)	1.55(4)
C(2)	0.3094(2)	−0.7301(2)	−0.4930(1)	2.82(5)
C(3)	0.2860(2)	−0.7241(2)	−0.5782(1)	3.11(5)

The structures were solved by the direct method and expanded using the Fourier technique. The non-hydrogen atoms were anisotropically refined. Hydrogen atoms were included in the structure factor calculations and isotropically refined for **2** and **3** but not refined for **1**. The final cycle of the full-matrix least-squares refinement of **1**−**3** was based on 1067, 1130, and 1073 observed reflections ($I > 3.00\sigma(I)$) and 85, 134, and 140 variable parameters, respectively. The unweighted and weighted agreement factors of the forms $R = \sum||F_o| - |F_c||/\sum|F_o|$ and $R_w = [\sum w(||F_o| - |F_c||)^2/\sum F_o^2)]^{1/2}$ are used. The agreement factors R (R_w) of **1**−**3** were 0.035 (0.034), 0.019 (0.019), and 0.024 (0.022), respectively. Crystallographic parameters are summarized in Table 1. The final positional parameters of the non-hydrogen atoms of **1**−**3** with their estimated standard deviations are listed in Tables 2−4, respectively.

Neutral atom scattering factors were taken from Cromer and Waber.[45] Anomalous dispersion effects were included in F_c; the values for $\Delta f'$ and $\Delta f''$ were those of Creagh and McAuley.[46] The values for the mass attenuation coefficients were those of Creagh and Hubbel.[47] All calculations were performed using the teXsan crystallographic software package from the Molecular Structure Corp.[48]

Table 4. Atomic Coordinates and Equivalent Isotropic Thermal Parameters (Å^2) of Non-Hydrogen Atoms in $[Ni(tn)_2]_3[Fe(CN)_6](ClO_4)_2$ (**3**)

atom	x	y	z	B(eq)
Ni	$^1/_2$	$-^1/_2$	$-^1/_2$	1.92(1)
Fe	0.6667	−0.6667	−0.6667	1.31(1)
Cl	1.0000	0	−0.6543(1)	4.37(2)
O(1)	1.0000	0	−0.5751(6)	13.5(2)
O(2)	0.9048(6)	−0.0176(7)	−0.6262(6)	13.8(4)
O(3)	1.0000	0	−0.732(1)	26.5(5)
O(4)	1.0732(5)	−0.0295(5)	−0.6837(4)	6.7(2)
N(1)	0.5195(2)	−0.6193(2)	−0.5633(1)	2.44(5)
N(2)	0.5431(2)	−0.4122(2)	−0.6045(1)	2.98(6)
N(3)	0.6649(2)	−0.4284(2)	−0.4721(2)	3.01(6)
C(1)	0.5722(2)	−0.6407(2)	−0.6021(1)	1.66(5)
C(2)	0.6302(3)	−0.2999(2)	−0.6028(2)	3.74(8)
C(3)	0.7332(2)	−0.3126(2)	−0.4882(2)	3.74(8)
C(4)	0.7342(3)	−0.2885(3)	−0.5730(2)	4.43(9)

Results and Discussion

Syntheses and General Properties. In our first attempt to create the 3-D bimetallic assemblies, hexacyanoferrate(II), $[Fe(CN)_6]^{4-}$, was adopted as the building block. This is based on our expectation that the combination of $[Ni(L)_2]^{2+}$ and $[Fe(CN)_6]^{4-}$ in the 3:1 stoichiometry may result in a 3-D network of the cubic Fe_8Ni_{12} unit (see Chart 1) whose cavity is large enough to accommodate two uninegative counterions required for neutralizing the dipositive charge per the cubic unit. As the counteranion, hexafluorophosphate or perchlorate ion was chosen. Ethylenediamine (en) or trimethylenediamine (tn) was utilized as the diamine ligand of $[Ni(L)_2]^{2+}$, because such a symmetric diamine may be preferred to asymmetric diamines such as 1,2-propanediamine (pn) and *N*-methylethylenediamine (N-men) in constructing the 3-D network based on the symmetric Fe_8Ni_{12} cube. Tris(diamine)nickel(II), $[Ni(L)_3]^{2+}$, was used for the synthesis of the bimetallic assemblies. In this synthesis, $[Ni(L)_3]^{2+}$ was gradually dissociated into $[Ni(L)_2]^{2+}$ in the aqueous solution, leading to the slow growth of single crystals of **1**−**3** suitable for the X-ray crystallographic study.

Each bimetallic assembly shows a sharp ν_{CN} peak at 2060 cm^{-1}. The ν_{CN} band is shifted to high frequency relative to that of $K_4[Fe(CN)_6]$ (2040 cm^{-1}). Such a shift of ν_{CN} mode and the appearance of only one ν_{CN} vibration suggest that all of the six cyanide groups of $[Fe(CN)_6]^{4-}$ are involved with the bridge to $[Ni(L)_2]^{2+}$. The IR spectra of **1**−**3** are essentially similar to each other except for the vibrations of the respective counteranion (PF_6^-, 860 and 560 cm^{-1}; ClO_4^-, 1100 and 620 cm^{-1}). All the assemblies are stable in air and insoluble in most inorganic and organic solvents.

Crystal Structures. The bimetallic assemblies **1**−**3** crystallize in the same trigonal crystal system of the space group $R\bar{3}$ (No. 148) and have very similar crystal parameters (Table 1). However, a significant difference is seen in the lattice parameters between the en compound **1** and tn compounds **2** and **3**.

$[Ni(en)_2]_3[Fe(CN)_6](PF_6)_2$ (1). The perspective view of the asymmetric unit with an atom-numbering scheme and the projection of the molecular entity in the lattice are shown in Figures 1−3. The selected bond distances and angles with their estimated standard deviations are listed in Table 5.

The asymmetric unit consists of a $^1/_6$ $[Fe(CN)_6]^{4-}$ anion, a $^1/_2$ *trans*-$[Ni(en)_2]^{2+}$ cation, and a $^1/_3$ PF_6^- anion. Hexacyanoferrate(II) coordinates to six $[Ni(en)_2]^{2+}$ cations through all its cyano nitrogens, forming a 3-D network structure extended by

(45) Cromer, D. T.; Waber, J. T. In *International Tables for X-Ray Crystallography*; The Kynoch Press: Birmingham, England, 1974; Vol. IV.
(46) Creagh, D. C.; McAuley, W. J. In *International Tables for Crystallography*; Kluwer Academic Publishers: Boston, MA, 1992; Vol. C.
(47) Creagh, D. C.; Hubbell, J. H. in *International Tables for Crystallography*; Kluwer Academic Publishers: Boston, MA, 1992; Vol. C.

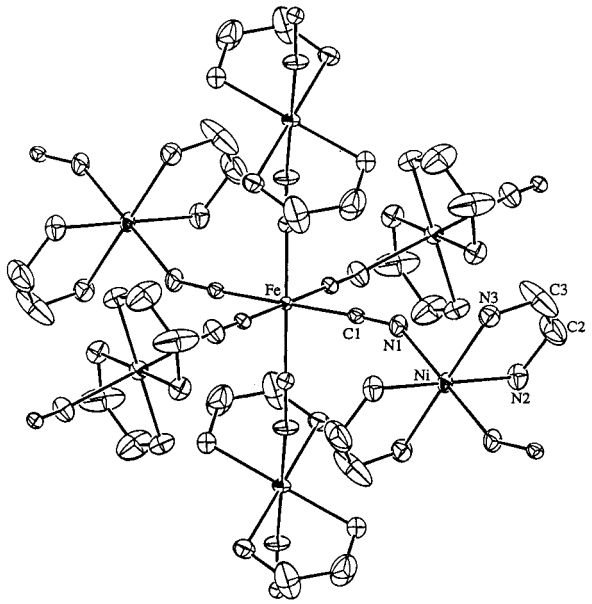

Figure 1. ORTEP drawing of the asymmetric unit of $[Ni(en)_2]_3[Fe(CN)_6](PF_6)_2$ (**1**) with the atom-labeling scheme, showing 30% probability ellipsolids.

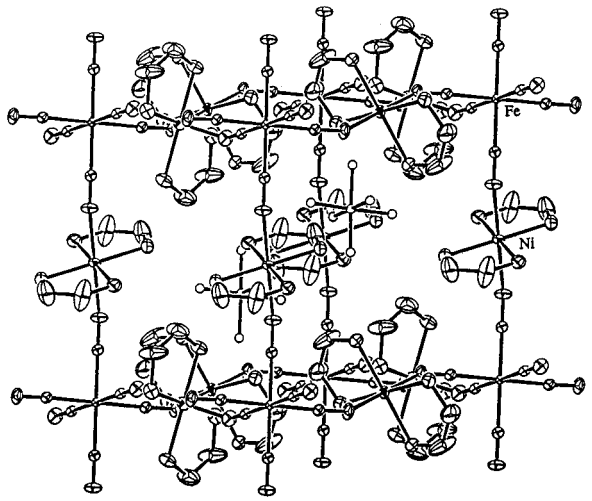

Figure 2. Structure of the Fe_8Ni_{12} cubic unit of **1**.

Table 5. Selected Bond Distances (Å) and Angles (deg) for **1**−**3**

compd	Fe−C(1)/Å	C(1)−N(1)/Å	Ni−N(1)/Å	C(1)−N(1)−Ni/deg
1	1.913(4)	1.152(4)	2.104(3)	148.2(3)
2	1.936(2)	1.163(2)	2.160(2)	151.7(2)
3	1.930(2)	1.160(3)	2.164(2)	149.3(2)

Fe^{II}−CN−Ni^{II} linkages (Figure 1). The Fe−C, C−N, and N−Ni bond distances in the linkage are 1.913(4), 1.152(4), and 2.104(3) Å, respectively. The Fe^{II}−C distance is significantly shorter than the Fe^{III}−C distances in the related assemblies because of strong π back-donation in the former; the mean Fe^{III}−C distance is 1.976 Å in $PPh_4[Ni(pn)_2][Fe^{III}(CN)_6]\cdot H_2O$,[11] 1.940 Å in $[Ni(en)_2]_3[Fe^{III}(CN)_6]_2\cdot 2H_2O$,[9,14] and 1.946 Å in $[Ni(pn)_2]_2[Fe^{III}(CN)_6]ClO_4\cdot 2H_2O$.[10−13] The CN−Ni bridging angle is 148.2(3)°. A cubic Fe_8Ni_{12} unit is formed by 8 $[Fe(CN)_6]^{4-}$ anions at the corners and with 12 $[Ni(en)_2]^{2+}$ cations at the edges (Figure 2). The nearest Fe···Ni, Fe···Fe, and Ni···Ni separations along the Fe−CN−Ni linkage are 4.954, 9.908, and 9.908 Å, respectively. The nearest Ni···Ni separation through space is 6.868 Å. Two hexafluorophosphate anions are located in the cavity of the Fe_8Ni_{12} cube. Two $[Fe(CN)_6]^{4-}$ and two PF_6^- anions align along the longest diagonal line (which coincides with the crystal *c* axis) of the Fe_8Ni_{12} cube. The PF_6^- and $[Fe(CN)_6]^{4-}$ ions in the same O_h symmetry are in the "eclipsed" mode with respect to the C_3 axis when projected onto the *ab* plane (Figure 3). The ethylenediamine entities play a role in filling the large cavity together with the PF_6^- ions.

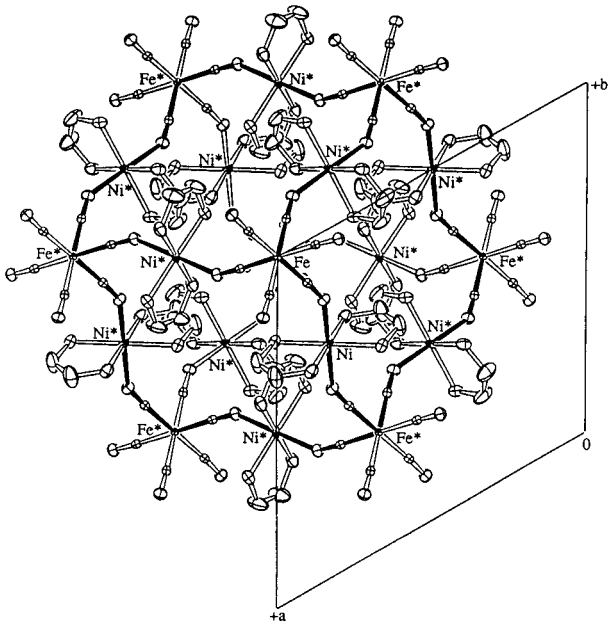

Figure 3. Projection of the polymeric structure of **1** onto the *ab* plane.

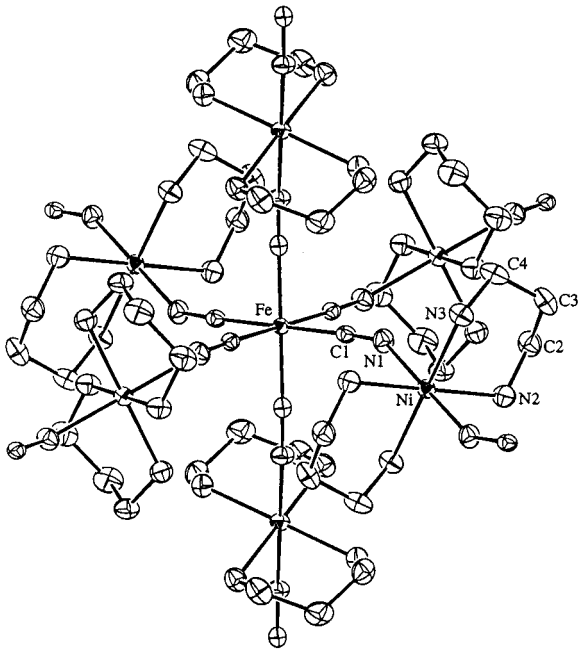

Figure 4. ORTEP drawing of the asymmetric unit of $[Ni(tn)_2]_3[Fe(CN)_6](PF_6)_2$ (**2**) with the atom-labeling scheme, showing 30% probability ellipsolids.

$[Ni(tn)_2]_3[Fe(CN)_6](PF_6)_2$ (2). The perspective view of the asymmetric unit with an atom-numbering scheme is given in Figure 4. Similar to the case of **1**, hexacyanoferrate(II) coordinates to six $[Ni(tn)_2]^{2+}$ cations through its six cyanide nitrogens, providing a 3-D network based on Fe_8Ni_{12} cubic units (Figures 5 and S1). The selected bond distances and angles are listed in Table 5. The trimethylenediamine in $[Ni(tn)_2]^{2+}$ assumes a chair conformation affording an inversion center at the Ni atom. The alignment of the $[Fe(CN)_6]^{4-}$ and PF_6^- ions in eclipsed mode is seen along the crystal *c* axis. The tn

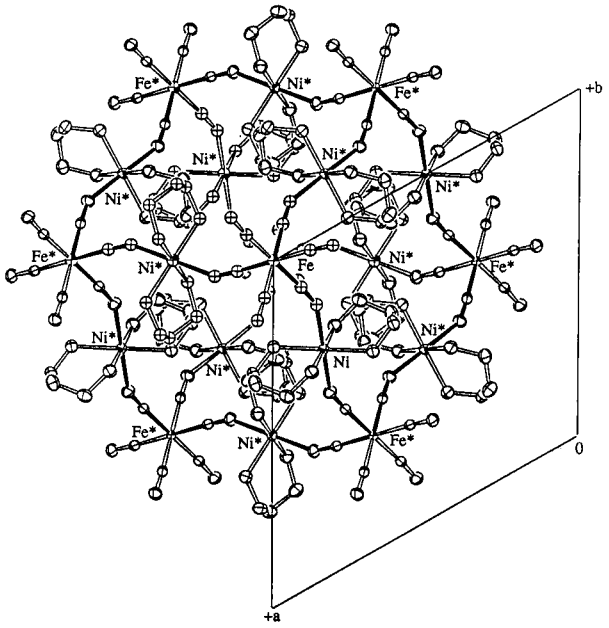

Figure 5. Projection of the polymeric structure of **2** onto the *ab* plane.

moieties play a role in filling the cubic cavity more effectively than the en moieties in the case of **2**.

$[Ni(tn)_2]_3[Fe(CN)_6](ClO_4)_2$ (3). The assembly **3** bears a marked resemblance to **2** in both the crystal structure of the asymmetric unit and the bulk structure (Figure S2). The selected bond distances and angles are listed in Table 5. Two perchlorate ions exist in the Fe_8Ni_{12} cube, aligning along *c* axis. The perchlorate oxygen atoms show large thermal parameters owing to a disorder along the *c* axis.

The cubic unit structures of **1**−**3** are comparatively studied in some detail. It is found from Table 5 that the structural data vary with the diamine ligand and counteranion. The tn compounds **2** and **3** have longer Fe−C and Ni−N bonds and a larger C−N−Ni angle compared with the en compound **1**. This may be attributed to an intramolecular steric strain that is larger in **2** and **3** with a tn ligand than in **1** with an en ligand. In comparison between **2** (with PF_6^-) and **3** (with ClO_4^-), **2** has larger lattice parameters than **3**. This is because **2** has large PF_6^- ions relative to the ClO_4^- ion in the cavity. The Fe−C and C−N bonds for **3** are evidently short relative to those for **2** whereas the Ni−N bond for **3** is long relative to that for **2**. It is to be noted that **1** has large equivalent isotropic thermal parameters with respect to the carbon atoms (C(2) and C(3)) of the ethylenediamine. The two enantiomeric conformations (λ and δ) of the ethylene group in $[Ni(en)_2]^{2+}$ can exist, and the large thermal parameters observed mean a disorder of the ethylene carbons with respect to the enantiomeric conformations. On the other hand, the tn ligand in **2** and **3** adopts a fixed chair conformation (Figure 6).

Magnetic Properties. The cryomagnetic properties of **1** and **2** are given in Figures 7 and 9, respectively, in the form of the $\chi_M T$ *vs* *T* plot.

$[Ni(en)_2]_3[Fe(CN)_6](PF_6)_2$ (1). At room temperature, the $\chi_M T$ value is 3.50 cm^3 K mol^{-1} (5.29 μ_B per $FeNi_3$) which is slightly larger than the expected value for the three high-spin Ni(II) ($S = 1$) ions (3.00 cm^3 K mol^{-1}, 4.90 μ_B). The $\chi_M T$ value is practically independent of temperature in the range 120−300 K but gradually increases with further decreasing temperature up to the maximum value of 5.05 cm^3 K mol^{-1} (6.34 μ_B) at 2.0 K. The $1/\chi_M$ vs *T* plots in the range 2.0−120 K obey the Curie−Weiss law with a positive Weiss constant of $\Theta = +1.16$ K

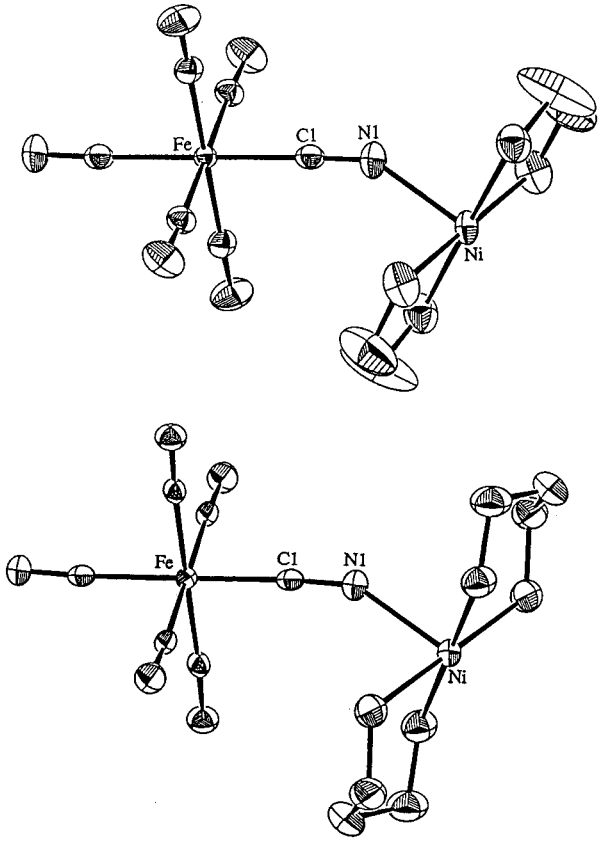

Figure 6. Bridging structures of **1** (above) and **2** and **3** (below).

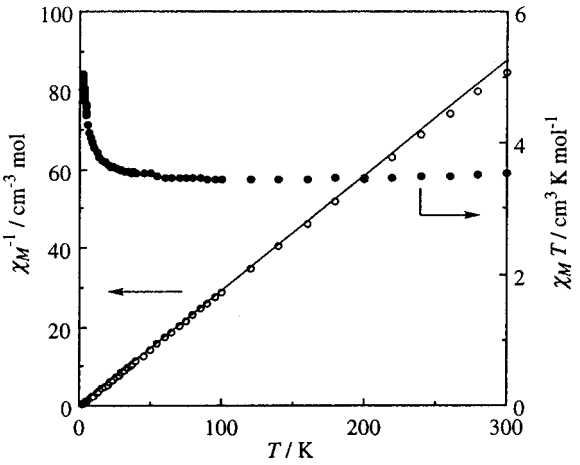

Figure 7. Plot of the temperature dependence of the $\chi_M T$ for **1** (per $FeNi_3$).

(based on $1/\chi_M = C(T - \Theta)$). The magnetic behavior below 120 K means a weak ferromagnetic interaction between the nearest Ni(II) ions through the −NC−Fe−CN− bridge. If one takes into consideration the electronic configurations of Ni(II) ($t_{2g}^6e_g^2$) and Fe(II) (t_{2g}^6), a σ-superexchange pathway is proposed between the nearest Ni(II) ions through the empty d_σ orbital of the Fe(II) ion. On the basis of this presumption and using the concept developed by Goodenough, Kanamori, and Anderson, an electron spin of the same sign as that of the unpaired electron on the d_{z^2}(Ni) orbital is polarized on the d_{z^2}(Fe) orbital (*z* axis is taken along the Ni−NC−Fe linkage) through the filled orbital of the cyanide bridges. This leads to a ferromagnetic coupling between the nearest Ni(II) ions through the diamagnetic Fe(II) ion.

The ferromagnetic behavior of **1** has been confirmed by the field dependence of magnetization measured at a temperature

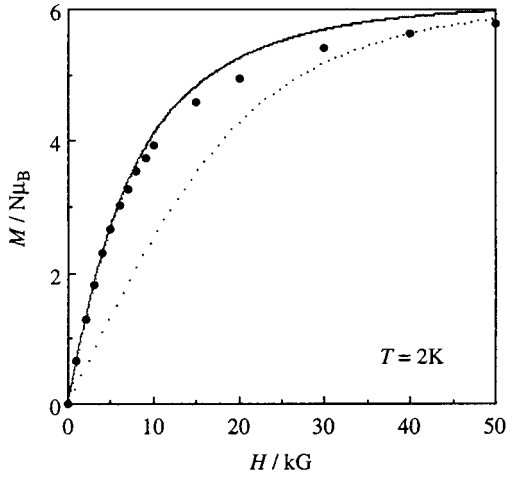

Figure 8. Field dependence of the magnetization at 2 K for **1** (per $FeNi_3$).

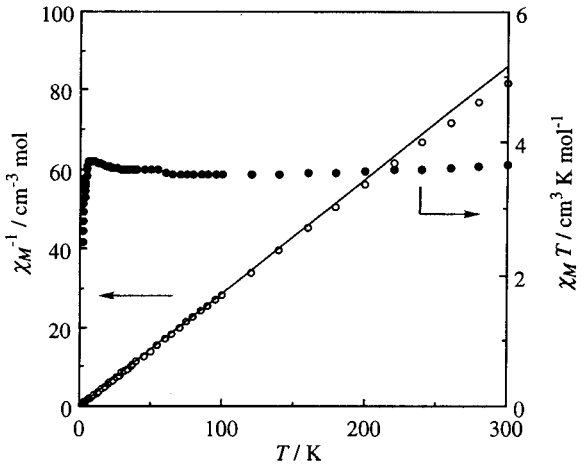

Figure 9. Plot of the temperature dependence of the $\chi_M T$ for **2** (per $FeNi_3$).

(2 K) corresponding to the maximum in the $\chi_M T$ vs T plots (Figure 8). The magnetization per Ni_3Fe at 50 kG is 5.77 $N\mu_B$ which is close to 6 $N\mu_B$, suggesting that all the spins in the Ni(II) ions aligned in pararell at high field. The dotted curve in Figure 8 shows the calculated magnetization based on the Brillouin function for three isolated $S = 1$ spins with $g = 2.02$. It is seen that the observed magnetization (per Ni_3Fe) is larger than the value predicted from the Brillouin function for three Ni(II) ions in the range of the applied field of 0−30 kG.

The field dependence of magnetization is interpreted using the mean-field approximation.[49,50] The theoretical magnetization is obtained by solving the following equations:

$$M = Ng\mu_B SB_s(x) \tag{1}$$

$$x = \frac{g\mu_B S(H + \lambda M)}{kT} \tag{2}$$

Here λ describes the magnitude of the internal field and can be represented as

$$\lambda = \Theta/C \quad C = \frac{Ng^2\mu_B{}^2 S(S+1)}{3k} \tag{3}$$

and eq 2 is expressed as follows:

$$x = \frac{g\mu_B SH}{kT} + \frac{3\Theta}{g(S+1)TN\mu_B}M \tag{4}$$

By the solution of eqs 1 and 4 for each magnetic field H, the theoretical curve with Weiss constant $\Theta = +1.16$ K is obtained and shown as the solid line in Figure 8. The calculated curve shows a shape similar to the observed one below 10 kG. In the high magnetic field, the observed value is slightly smaller than the theoretical one, which is due to the magnetic anisotropy of the Ni(II) ion. This result below 10 kG is a strong indication of the ferromagnetic interaction between the nearest Ni(II) ions through the −NC−Fe−CN− bridge.

$[Ni(tn)_2]_3[Fe(CN)_6](PF_6)_2$ (2). The magnetic behavior of **2** in the range of 120−300 K is essentially the same as that of **1**. Below 100 K, the $\chi_M T$ value of **2** increases with decreasing temperature to a maximum value of 3.73 cm^3 K mol^{-1} at 8.0 K (5.46 μ_B) which is slightly larger than the expected value for three Ni(II) ($S = 1$) ions. This fact suggests a ferromagnetic interaction between the nearest Ni(II) ions. The $1/\chi_M$ vs T plots in the range of 8.0−100 K obey the Curie−Weiss law with a small positive Weiss constant of $\Theta = +0.80$ K. The χ_M value also increases with decreasing temperature up to the maximum value at 2 K. It is found that the maximum $\chi_M T$ value of **2** is small compared with that of **1**. Furthermore, the $\chi_M T$ of **2** rapidly decreases with decreasing temperature below 8 K probably due to zero-field splitting for the Ni(II) ion. Such a zero-field effect is not prominent in the cryomagnetic property of **1**. This means that the ferromagnetic interaction between the nearest Ni(II) ions is more dominant than the zero-field effect of Ni(II) in **1**, whereas is less effective in **2**. The weak ferromagnetic interaction in **2** may be related to the elongated Fe−CN−Ni distance as will be discussed later.

The field dependence of magnetization for **2**, measured at the temperature (8 K) corresponding to the maximal $\chi_M T$ in the $\chi_M T$ *vs* T plots, is shown in Figure 10. This result indicates that the ferromagnetic interaction between the nearest Ni(II) ions is too weak to be saturated at 8 K even under a large applied field of 50 kG. Noteworthy is the fact that the magnetization of **2** exceeds the value predicted from the Brillouin function for three isolated $S = 1$ spins over the applied-field range studied (Figure 10). This fact adds support to the fact that the nearest Ni(II) ions are ferromagnetically interacting through the −NC−Fe−CN− bridge.

$[Ni(tn)_2]_3[Fe(CN)_6](ClO_4)_2$ (3). The magnetic behavior of **3** is similar to that of **2**. Below 100 K, the $\chi_M T$ value slightly increases with decreasing temperature up to the maximum value of 3.88 cm^3 K mol^{-1} at 8.0 K (5.57 μ_B) and rapidly decreases below 8 K probably due to zero-field splitting for the Ni(II) ion. This behavior suggests that a ferromagnetic interaction operates between the nearest Ni(II) ions but the magnetic interaction is less effective than the zero-field effect of the Ni(II) ion. The $1/\chi_M$ vs T plots in the range of 8.0−100 K obey the Curie−Weiss law with a positive Weiss constant of $\Theta = +0.82$ K. The Weiss constant is comparable to but slightly larger than that for **2** ($\Theta = +0.80$ K).

Thus, all the assemblies **1**−**3** show a ferromagnetic interaction between the nearest Ni(II) ions but no three-dimensional magnetic ordering occurs over the lattice. The ferromagnetic interaction becomes stronger in the order **1** > **3** ≥ **2**. This order

(48) teXsan: Crystal Structure Analysis package, Molecular Structure Corp., 1985, 1992.
(49) Veciana, J.; Rovira, C.; Ventosa, N.; Crespo, M. I.; Palacio, F. *J. Am. Chem. Soc.* **1993**, *115*, 57.

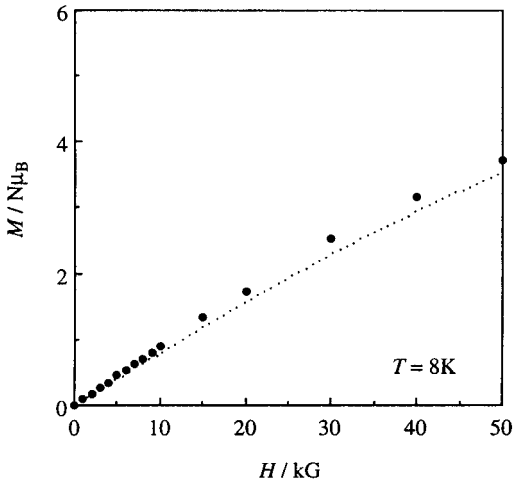

Figure 10. Field dependence of the magnetization at 8 K for **2** (per $FeNi_3$).

is in accord with the increasing order of the Fe−C(1) and Ni−N(1) bond distances, **1** (1.913, 2.104 Å) < **3** (1.930, 2.163 Å) ≤ **2** (1.936, 2.160 Å). Such an elongation of bond distances means a decreasing overlap integral among their d_σ orbitals and is unfavorable for the magnetic interaction between Ni(II) ions through diamagnetic Fe(II) ion.

The substitution of the diamagnetic Fe(II) ion for a paramagnetic ion is of great interest in achieving a long-range magnetic ordering over the 3-D lattice. Studies along this line are in progress in our laboratory.

(50) Matsuda, K.; Nakamura, N.; Inoue, K.; Koga, N.; Iwamura, H. *Bull. Chem. Soc. Jpn.* **1996**, *69*, 1483.

Conclusion

Three 3-D bimetallic assemblies of the general formula $[Ni(L)_2]_3[Fe^{II}(CN)_6]X_2$ ((L, X) = (en, PF_6^-) (**1**), (tn, PF_6^-) (**2**), (tn, ClO_4^-) (**3**)) have been obtained from the reaction of $[Ni(L)_3]X_2$ and $K_4[Fe(CN)_6]$. X-ray crystallography for the assemblies reveals a 3-D network structure extended by the Fe−CN−Ni−NC−Fe linkages. The network is based on the Fe_8Ni_{12} cubic unit with Fe(II) ions at the corners of the cube and Ni(II) ions at the middle of the edges. They are the first example of 3-D bimetallic assemblies derived from $[M(CN)_6]^{n-}$ and planar $[Ni(L)_2]^{2+}$.

Cryomagnetic studies reveal a ferromagnetic spin-exchange between the nearest Ni(II) ions through the diamagnetic Fe(II) ion. This result corresponds to the specific properties of the second components in Prussian blue analogues. The ferromagnetic interaction decreases in the order **1** > **3** ≥ **2** which is in accord with the increasing order of the Fe−C(1) and Ni−N(1) bond distances, **1** < **3** ≤ **2**. No three-dimensional magnetic ordering occurs over the lattice down to 2 K due to the intervention of the diamagnetic $[Fe^{II}(CN)_6]^{4-}$.

Acknowledgment. This work was supported by a Grant-in-Aid for Scientific Research (No. 09740494) from the Ministry of Education, Science, and Culture of Japan.

Supporting Information Available: Structure of the Fe_8Ni_{12} cubic unit of **2** and a projection of the polymeric structure of **3** onto the *ab* plane (Figures S1 and S2) and tables of magnetic susceptibility and magnetization data for **1**−**3** (9 pages). Three X-ray crystallographic files, in CIF format, are available. Ordering and/or access information is given on any current masthead page.

IC9711168